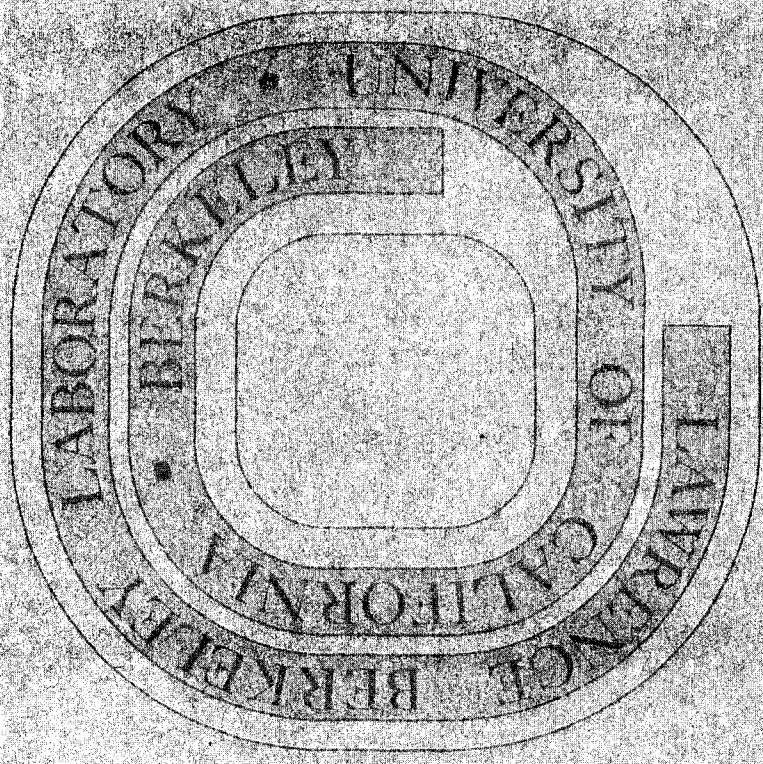

Submitted to Physical Review

UNIVERSITY OF CALIFORNIA
Lawrence Radiation Laboratory
Berkeley, California

UCRL-11537 Rev.

AEC Contract No. W-7405-eng-48

π^+-p SCATTERING AT 250 MeV: EXPERIMENT AND ANALYSIS

Wladyslaw Troka, Fred Betz, Owen Chamberlain, Byron Dieterle,
Helmut Dost, Claude Schultz, and Gilbert Shapiro

May 1965

π^+-p Scattering at 250 MeV: Experiment and Analysis*

Wladyslaw Troka, Fred Betz, Owen Chamberlain, Byron Dieterle,
Helmut Dost, Claude Schultz, and Gilbert Shapiro
University of California
Lawrence Radiation Laboratory, Berkeley

May 1965

ABSTRACT

The differential cross section for elastic scattering of positive pions on protons has been measured at a nominal incident-meson kinetic energy of 250 MeV. The angular range covered in the center of mass by the 13 data points was 14.9 deg to 160 deg. The fractional rms errors were typically 1.5%. A liquid hydrogen target was bombarded by a beam of 2.5×10^6 mesons/sec. The scattered pions were detected by a counter telescope. Recoil protons were eliminated by means of a Cerenkov counter.

A phase-shift analysis was performed combining the above-mentioned data with the recoil-proton polarization measurements taken recently with the help of a polarized proton target. Only one acceptable SPD Fermi-type phase-shift set was found. When F waves were included, a total of three possible phase-shift solutions emerged from the analysis. However, arguments based on the data could still be made to eliminate all but one phase-shift set. On the other hand, the remaining phase-shift set, similar in type to the SPD solution, suffers from the disadvantage of large rms errors assigned to its small phase shifts.

I. INTRODUCTION

Although a considerable number of measurements exist on π^+p scattering, they are seldom ever complete or precise. The primary cause of low accuracy in many experiments was that high-intensity pion beams were not available. The most complete work up to date on π^+p scattering exists at 310 MeV.[1,2] The total cross section, differential cross section, and recoil-

proton polarization were measured at his energy.

This report represents part of an effort to extend this completeness to a lower energy. In this experiment we have measured the differential cross section with typically 1.5% fractional rms errors at 250 MeV nominal incident-meson kinetic energy. The measurement of the recoil-proton polarization was accomplished in a companion experiment,[3] at the same incident-meson kinetic energy.

The analysis of the scattering data was carried out by the method of partial waves. The maximum orbital angular momentum quantum number L_{MAX} of the partial wave expansion must be determined empirically at present. The results of $L_{MAX} = 2$ and $L_{MAX} = 3$ phase-shift analyses are presented in this report.

Inelastic scattering was neglected in the analysis. The error committed should be negligible when one compares the estimated 0.2-mb total inelastic cross section with 110 mb for the total elastic cross section at 250 MeV.

II. PION BEAM

Figure 1 shows the plan view of the beam spectrograph. Positive pions were produced by inserting a polyethylene target into the external proton beam of the 184-in. cyclotron. The proton energy and intensity at the target were 745 ± 8 MeV and (2 ± 1) x 10^{11} protons/sec respectively. The length of the production target was optimized at 30.5 in. for maximum meson yield at central momentum of the spectrograph (363.5 MeV/c).

Pions produced in the forward direction were first momentum-analyzed by the bending magnet M1 , then brought to an intermediate focus at the physical center F1 of the three-section quadrupole magnet Q. Because of the momentum dispersion of M1 , the off-momentum foci were laterally displaced from the center of Q. Therefore, momentum definition was obtained by placing a slit here. In this case there was a 2-in.-wide aperture which corresponded to a momentum spread of ±3%. Protons of the central momentum were degraded by a 1-in. polethylene absorber placed near the intermediate focus and swept out of the main beam by the bending magnet M2 . The spectrograph was symmetrical about the first focus. The second half approximately cancelled the momentum dispersion of the first half. An evacuated

can was placed inside the magnet system to minimize Coulomb scattering of the beam.

The emerging pion beam at the second focus F2, where the hydrogen target was located, was about 2 in. wide and 1.5 in. high at the half-maximum points. The measured beam divergence at the half-maximum points was ± 2 deg. A maximum beam intensity of 2.5×10^6 mesons/sec was measured by using an argon-filled ionization chamber. A three-counter range telescope with a variable copper absorber between the last two counters was set up repeatedly during the experiment to check on the energy of the pions at the center of the hydrogen target. The mean energy for the experiment was found to be 247.5 MeV with an rms uncertainty of ± 1.5 MeV. Muons, the main beam contaminant, were estimated at about 5% of all beam particles. The percentage of positrons was judged to be considerably smaller than that. Knowledge of the exact numbers of these beam particles was not necessary here, because only a relative cross-section measurement was made.

III. DIFFERENTIAL CROSS-SECTION MEASUREMENT

A. Experimental Apparatus

Figure 2 is a schematic drawing of the two counter telescopes used during the experiment. They are shown at a typical angular setting with respect to the incident beam direction.

The counters are listed in Table I. The telescope on the right in Fig. 2, normally counting pions, consisted of four counters. The scintillation counter S_2 defined the solid angle of the telescope.

Located directly behind S_2 was a water Cerenkov counter C designed to eliminate recoil protons by only counting charged particles with velocities $\beta > 0.75$. The relatively large thickness of this counter was chosen to assure a reasonable detection efficiency, even for lab angles near 180 deg. Some distance in front of S_2 was another scintillation counter, S_1. Its purpose was to reduce the solid angle of the telescope for particles that did not originate in hydrogen. Finally, at a distance of 10 in. behind S_2 (to allow room for some carbon absorber), there was an auxiliary scintillation counter S_3. It was used for range curves of the scattered beam and

in the measurement of the Cerenkov-counter efficiencies.

For laboratory-system angles equal to or larger than 22.3 deg the solid angle defined by S_2 was $\Omega = 0.265 \times 10^{-2}$ sr. This counter geometry will be called SA (short arm). At angles smaller than 22.3 deg, the telescope with the dimensions shown in Fig. 2 would count too many pions of the incident beam that did not scatter in the hydrogen target. In order to keep this background tolerable, S_2 and the other counters of the pion telescope were moved fartheraway from the target center. This counter geometry will be referred to as LA (long arm).

The telescope on the left of Fig. 2, normally counting protons in coincidence with the pion telescope, consisted of two scintillation counters, S_4 and S_5. Their sizes and distances from the hydrogen target were chosen on the basis of the proton-to-pion solid-angle ratio with due regard to the large multiple Coulomb scattering of the slower recoil protons. S_4 and S_5 were used only during the measurement of the Cerenkov efficiencies.

The ionization chamber was used to monitor the incident beam. Two scintillation counters, which are not shown in Fig. 2 were located some distance off the scattering plane to monitor the scattered beam.

Liquid hydrogen was contained in a 3-in.-diameter 6-in. long upright cylinder made of 0.0075-in. Mylar. To reduce heat transfer the flask was surrounded by a 6-in.-diameter vacuum jacket consisting of a Mylar-wrapped 0.061-in.-thick aluminum can. Four-in. holes were cut into the aluminum can along the beam line to reduce the non-hydrogen interactions (flask-empty rate). A check was made on the actual position of the flask within the vacuum jacket. X-ray photographs of the hydrogen target both with full and with empty flask showed no measurable eccentricity.

B. Experimental Method

1. Cerenkov efficiencies. The efficiency for pions was expected to vary rapidly with pion velocity. Therefore, it was measured at most of the

same laboratory-system angles as the differential cross section. Below 90 deg lab, the upper kinematic limit for recoil protons, hydrogen-scattered pions were selected by counting in coincidence with conjugate protons. This arrangement is seen in Fig. 2. The efficiency was determined by taking the ratio of coincidences $S_1S_2S_3S_4S_5C$ to $S_1S_2S_3S_4S_5$, after background subtraction. Laboratory-system angles smaller than about 45 deg could not be covered by this method, because too many conjugate protons were stopping in the target walls. For angles larger than 90 deg the pion-efficiency measurements were continued by recording the ratio of coincidences $S_1S_2S_3C$ to $S_1S_2S_3$, again after background subtraction. The same scheme was also used to get a reference point at the incident pion energy.

Since recoil protons could cause scintillation, either in water or the surrounding magnesium oxide, the detection efficiency for protons had to be determined also. Furthermore, recoil protons could produce fast electrons by knock-on, which in turn could have been the source of unwanted Cerenkov light. The measurement was made by reversing the roles of the two counter telescopes. The pion telescope was counting protons and the proton telescope counted the conjugate mesons. As before, the ratio of sixfold to fivefold coincidences was recorded.

2. Scattering data. Our desire to obtain an accurate angular distribution for pion-proton scattering conflicted with some of the requirements of an absolute measurement of differential cross section. Therefore, we decided to restrict this work to the measurement of the relative differential cross section ("angular distribution"). Then, before our data were directly useful, they had to be fitted to total cross-section values taken from other experimental work.

The angular distribution was measured at thirteen angular positions between 14.9 deg and 160 deg in the center-of-mass system.

The number of incident pions in the beam was measured by allowing an ionization chamber to deposit its charge on a capacitor and recording the capacitor potential I_0 in volts. I_0 is then used as a constant proportional to the number of incident pions in the beam in any given beam exposure. $I(\theta)$, the number of pions scattered into the solid angle of the counter telescope, was detected by the coincidence S_1S_2C. The contribution from the target

walls was eliminated by taking the difference between target-full and target-empty rates. The ratio of the background to the hydrogen effect varied for most angles between 0.3 and 0.5. Only the most forward angles of 14.8 deg and 11.0 deg lab had the exceptionally high ratios of 1.6 and 5.8 respectively.

Many precautions were taken to search for and minimize systematic errors. The incident beam was scanned periodically to center it on the target. Also, range curves of the incoming particles were often examined to maintain a constant pion energy at the center of the target. Finally, except at very small and very large angles, scattered pions were counted to the left and right of the incident beam direction. At 22.3 deg, the smallest angle at which this method was feasible, the difference between the left and right averages was only 1.7% for the hydrogen effect, although the left background was almost twice the right background. This difference was not significant considering the error assigned to the data at this angle. In order to detect systematic drifts in the scattering data, measurements were returned repeatedly to a check angle established at 37.7 deg. Consistency plots at this angle showed no systematic changes. A running check was kept with stationary monitors to detect differences between successive flask-full or flask-empty conditions. Only normal fluctuations were found. Part of the raw data was collected at about 1/5 of full beam because of safety requirements imposed by nearby construction. Intermediate changes in the beam level were also introduced deliberately at 22.3 deg. No significant differences indicating a rate dependence were observed. An estimate of the accidental rate for a threefold coincidence was obtained by delaying the output from S_3 by 52×10^{-9} sec and combining it with S_1 and S_2. This delay corresponds to the separation between rf pulses of the Berkeley cyclotron. The accidental rate was never larger than 0.3% of the scattered pion rate. The performance of the electronic components was also checked. Counter voltage plateaus and relative delays were examined repeatedly.

IV. DATA REDUCTION

A. Corrections

A variety of corrections was necessary to account for the departure from the ideal case, in which the differential cross section is exactly proportional to the net (S_1S_2C) coincidence rate. Some pions were lost by second nuclear scattering in hydrogen itself, in the target walls, and in the counters of the pion telescope. Then, because of the sizable separation of the defining counter from the target, some pions decayed in flight. The efficiency of the Cerenkov, less than 100%, caused a further reduction in the counting rate of the scattered pion flux. Finally, there was a small geometrical correction due to the finite target volume and finite detector area.

Application of these corrections to the basic (S_1S_2C) rate yields, for the differential cross section, the expression

$$\frac{d\sigma}{d\Omega} = \frac{(1-f_p)\ (S_1S_2C)_{NET}}{(1-f)\epsilon\ g\ I_o'\ N(\Delta\ \Omega)} \quad , \qquad (1)$$

where $(S_1S_2C)_{NET}$ represents the background-subtracted number of three-fold coincidences, normalized to ion-chamber volts; and f_p is the number of protons counted by the Cerenkov, expressed as a fraction of the total rate in this counter. The fraction of pions lost by second nuclear scattering and pion decay is given by f (higher-order scattering was neglected); ϵ is a generalized efficiency of the Cerenkov counter, calculated for scattered particles other than protons; g represents the geometrical correction. Not shown explicitly is a small correction applied at the two most forward angles to compensate for the attenuation of the background by the target hydrogen.

The remaining factors are: I_o' , the number of incident pions per ion-chamber volt; N , the number of proton scatterers per cm^2; and $\Delta\ \Omega$, the solid angle of the pion telescope. These normalizing factors are independent of the scattering angle. Knowledge of their exact magnitude was not necessary, because the normalization (to mb/sr) was obtained from a previously known total cross section by integration.

A summary of the experimental data with its corrections is given in Table II.

B. Normalization and Results

The normalization of the corrected data to mb/sr was obtained in the following way. In the first step, the one-level resonance formula by Gell-Mann and Watson[4] was fitted to a set of 50 experimental total cross-section values, between 33 MeV and 550 MeV pion kinetic energy. Applying the best fit we calculated a total cross section

$$\sigma_{TOT} = 114.5 \pm 2.9 \text{ mb} \qquad (2)$$

at 247.5 MeV incident-pion kinetic energy.

The data closest to the energy of the present experiment were those of Mukhin et al.[5] at 240 MeV. From the comments in their paper we deduced that we could take the value of the total cross section measured with a c.m. meson cutoff angle θ_c^* of 11 deg (and a corresponding cutoff angle $\theta_c^{*'}$ for the protons) to be 5 ± 1.5 mb less than the value quoted by Mukhin et al. for 0 deg cutoff angle. We therefore adopted as the total cross section at 247.5 MeV with 11 deg c.m. meson cutoff angle a value 5 ± 1.5 mb less than that given in expression (2). We used, then,

$$\sigma_{TOT} = 109.5 \pm 3.3 \text{ mb} \qquad (3)$$

for 11 deg cutoff angle and incident-meson kinetic energy of 247.5 MeV. The corrected angular distribution and the phase-shift analysis were normalized to this value. The relative error above is 3%, which is also the uncertainty assigned to the absolute scale of the differential cross section.

The differential cross section is presented in Table III as a function of the center-of-mass scattering angle θ^*.

C. Errors

The basic component of the errors assigned to the differential cross section in Table III derives from counting statistics. This error was determined for a particular data point from the usual formula based on the Poisson distribution of the scattering events:

$$\Delta\left(\frac{I(\theta)}{I_o}\right) = \left[\frac{I(\theta)}{I_o^2}\Big|_{FULL} + \frac{I(\theta)}{I_o^2}\Big|_{EMPTY}\right]^{1/2} \qquad (4)$$

where I_o is the number of ion-chamber volts in a given beam exposure and $I(\theta)$ is the corresponding number of pions scattered into the solid angle of the counter telescope.

Considering the relatively high counting rates of this experiment, small counting errors, typically 1%, were the rule at practically all scattering angles. Therefore, systematic errors became very important. A considerable amount of effort was spent to calculate these errors and to obtain a realistic assessment of the uncertainties involved in their calculation. The errors assigned to the differential cross section include the estimated errors in all corrections. Most of the corrections were small, which minimized the effect of their uncertainties. The exception to this rule was the overall Cerenkov efficiency ϵ. However, it is well to note that the calculated part of this correction is roughly given by the difference between the overall Cerenkov-counter efficiency and the directly observed efficiency. This difference is about 2% for the forward angles and reaches 5.5% only for the backward angles. In the latter region comparison is possible with the directly measured doubles rate (S_1S_2), because recoil protons are absent here. The agreement between this rate and the bulk of the data derived from (S_1S_2C) was quite good. The (S_1S_2) data were therefore incorporated into the final results.

The agreement at the point of overlapping counter geometries (θ_{LAB} = 22.3 deg) was also satisfactory. This can be verified by reference to Table II.

V. PHASE-SHIFT ANALYSIS

Three distinct sets of data were used in the phase-shift analysis. In the first set were the 13 differential cross-section points given in Table III. The second set consisted of the recoil-proton polarization measured at seven scattering angles by our group.[3] The mean incident-meson kinetic energy of that experiment was 246/MeV, which is within one standard deviation of the mean energy of the differential cross-section measurement. The polarization data are shown in Table IV. Finally, there was the total cross-section at θ_c = 11 deg given in Eq. (3).

Part A describes the relationship between the experimental data and the phase shifts, and reviews the general features of the computer program which calculates the latter quantities. Part B presents the results of the analysis. A discussion of the results follows in Part C.

A. Partial-Wave Expansion

The connection between the differential cross section and the recoil-proton polarization on one hand, and the phase shifts on the other hand is usually expressed by means of the non-spin-flip scattering amplitude g and the spin-flip amplitude h[6]. The differential cross section for pions scattering from an unpolarized target is written

$$\frac{d\sigma}{d\Omega}(\theta) = |g(\theta)|^2 + |h(\theta)|^2 \quad , \tag{5}$$

where the star indicating a center-of-mass angle is omitted. All expressions in this section refer to the barycentric system only. The recoil-proton polarization is in turn written

$$P(\theta) = \frac{2\mathrm{Re}\, g^*(\theta)h(\theta)}{|g(\theta)|^2+|h(\theta)|^2} \tag{6}$$

Finally, neglecting Coulomb effects, the partial-wave expansions of the scattering amplitudes can be written

$$g(\theta) = \lambda\!\!\!^{-} \sum_{L=0}^{L_{MAX}} \left((L+1) \frac{\exp\left[2i\delta_L^{+}\right]-1}{2i} + L \frac{\exp\left[2i\delta_L^{-}\right]-1}{2i} \right) P_L(\cos\theta) \quad , \tag{7}$$

and

$$h(\theta) = \lambda\!\!\!^{-} \sum_{L=1}^{L_{MAX}} \left(\frac{\exp\left[2i\delta_L^{+}\right] - \exp\left[2i\delta_L^{-}\right]}{2} \right) P_L^{1}(\cos\theta) \quad . \tag{8}$$

Here, $\lambda\!\!\!^{-}$ is the wavelength divided by 2π ; L is the orbital angular-momentum quantum number; $P_L(\cos\theta)$ is the Legendre polynomial of order L ; $P_L^{1}(\cos\theta)$ is the associated Legendre polynomial of the same order. Finally, $\delta_L^{\pm}$ are the phase shifts for the orbital angular-momentum state

L and the total angular momentum quantum number $J = L \pm 1/2$. The isotopic spin quantum number is suppressed in this notation; it is 3/2 for the π^+-p system. The phase shifts $\delta_L^{\pm}$ in Eqs. (7) and (8) are real quantities, since inelastic scattering has been neglected.

Expressions similar to Eqs. (7) and (8) which include Coulomb corrections are given by Foote et al.[7]

The IBM 7090 program PIPANAL IV, developed by Foote,[7] was used in the analysis. The method of computation rests on the grid search method,[8] in which a trial set of phase shifts is varied by a steadily decreasing increment until a minimum of the quantity

$$\chi^2 = \sum_i \left[\frac{X_i^{(c)} - X_i^{(e)}}{\Delta X_i} \right]^2 \qquad (9)$$

is reached. Here, $X_i^{(e)}$ is the experimental value of the differential cross section, polarization or total cross section; ΔX_i is its experimental error. The corresponding quantity calculated by the program for a given set of phase shifts is given by $X_i^{(c)}$; the summation over the index i extends over all data points.

To establish the uncertainty in the set of phase shifts accompanying the minimum χ^2 , the program calculates the matrix elements

$$G_{ij} = \frac{\partial^2(\chi^2)}{\partial\delta_i \partial\delta_j} \quad , \qquad (10)$$

where the indices i, j range over the number of phase shifts δ . The errors assigned to the phase shifts are obtained from the diagonal elements of the inverse matrix G^{-1} (error matrix):[9]

$$\Delta\delta_i = \sqrt{(G^{-1})_{ii}} \quad . \qquad (11)$$

B. Results

1. SPD analysis. The notation of spectroscopy, S,P,D,F, etc., will be used from here on to denote the orbital angular momentum quantum number L = 0,1,2,3, etc. The subscripts 2T,2J will again indicate the isotopic spin and total angular momentum quantum numbers.

It was already apparent from the normalization of the differential cross section that D waves were necessary for an adequate fit. Thus, a SP analysis was omitted. Three hundred different sets of random phase shifts, ranging from -90 deg to +90 deg, were fed into the computer together with the data listed at the beginning of this section. Only one set of phase shifts fitted the differential cross-section and polarization data well. This solution is listed in Table V-1. under the label of Fermi-I (I means $D_{3,3}-D_{3,5} > 0$). Other solutions also appeared, but based on the χ^2 - distribution their likelihood of being the correct set was less than 1%.

2. SPDF analysis. It was decided to include F waves despite their expected small magnitude, because of the often-demonstrated sensitivity of the polarization data to the small phase shifts. This time, 240 initial sets of phase shifts were used as the starting points of the analysis. Again. these phase shifts were selected at random with the exception of the F phase shifts, which were set to zero.

The results, which are shown in Table V-2. are similar to those of Foote.[7] Although the SPDF counterpart of the SPD Fermi-I solution was found (solution A), two other solutions also emerged that had low χ^2. Solution B is of the Fermi I type. It has a very large $F_{3,7}$ phase shift, therefore, it can be neglected on this ground. Solution C is analogous to Footé's Fermi-II solution. On the basis of the χ^2 distribution alone it has less than a 5% chance of being the right solution. More convincing, perhaps, is the more than threefold increase in the χ^2 contribution from the polarization between solutions A and C. A qualitative argument can be made directly from the plot of the polarization data in Fig. 3, where the calculated polarizations based on the three SPDF solutions are shown. While the backward angles are equally well fitted by either solution, the two measurements at 60.8 and 80.5 deg clearly favor solution A. The conclusion is, therefore, that solution A best fits the polarization and differential cross-section data.

C. Discussion

At first sight, the SPDF results may look alarming as they did to Foote et al.,[7] who first attempted to extend the analysis to include F waves. The proper interpretation of the emergence of several solutions is the exhaustion of the information contained in the majority of the experimental data, namely, the differential cross section. This point is illustrated in Fig. 4, where the fits of solutions A and B are compared. (The fit of solution C is indistinguishable from that of solution A). A large $D_{3,5}$ phase shift of -24.6 deg, coupled with a 21.0 deg $F_{3,7}$ phase shift, makes only a small difference at the extreme forward and backward angles, where the accurate measurement of the differential cross section is exceedingly difficult in any case. The large increase in the errors assigned to the small phase shifts of solution A is another manifestation of this loss of resolution. Nevertheless, the magnitude of these errors is somewhat deceiving because of the large amount of correlation that exists between the phase shifts. Consequently, the error matrices of the acceptable SPD and SPDF solutions are also given in Table VI.

The agreement with other experiments, notably with Foote and Rogers, is good. The evidence which led to the rejection of solution C (Fermi-II) is substantiated by Vik and Rugge,[10] who performed a SPDF analysis at 310 MeV using data from π^--p elastic scattering, recoil-proton polarization, and charge-exchange scattering. These authors found no solution fitting all their data by starting the search from Foote's Fermi-II solution. Finally, the phenomenological analysis by Roper[11] predicts phase shifts at 247 MeV which are very close to those of solution A.

Comparison with theory is made only with the most recent work by Donnachie, Hamilton, and Lea,[12] which is based on dispersion relations for the partial-wave scattering amplitudes. Due to the method of their analysis, their predictions are valid only for $L \geqslant 1$, but they improve with increasing L. The results of these calculations are

$P_{3,1}$	$D_{3,3}$	$D_{3,5}$	$F_{3,5}$	$F_{3,7}$
-9.2 ± 0.8	-0.5 ± 0.2	-1.3 ± 0.1	-0.04 ± 0.04	0.34 ± 0.05

Solution A fits these predictions best.

Summarizing, while only one acceptable SPDF solution was found, no

claim can be made that the polarization and differential cross-section data alone, no matter how accurately measured, are capable of establishing the small phase shifts accurately. A proposal[13] has been advanced to measure the spin rotation coefficients, since they are capable of sensitive discrimination against the Fermi-II solution. However, technical difficulties will delay the measurement of these parameters for some time. Therefore, $\pi^- p$ scattering that involves both the isotopic-spin $T = 3/2$ and $T = 1/2$ states will in the near future remain the only source of accurate phase-shift analyses in the pion-nucleon system.

REFERENCES

* This work was done under the auspices of the U.S. Atomic Energy Commission

1. J. H. Foote, O. Chamberlain, E. H. Rogers, H. M. Steiner, C. E. Wiegand, and T. Ypsilantis, Phys. Rev. 122,948 (1961).

2. E. H. Rogers, Scattering of 310-MeV Positive Pions by Protons: Experiments and Analysis (Thesis) UCRL-10127, March 1962.

3. O. Chamberlain, C. D. Jeffries, C. H. Schultz, G. Shapiro, and L. Van Rossum, Physics Letters 7, 293 (1963)
C. H. Schultz, Scattering of 250-MeV Positive Pi Mesons from a Polarized Proton Target (Thesis), UCRL-11149, January 1964 (unpublished).

4. M. Gell-Mann, and K. M. Watson, Ann. Rev. Nucl. Sci. 4, 219 (1954).

5. A. I. Mukhin, E. B. Ozerov, B. M. Pontecorvo, E. L. Grigoriev, and N. A. Nitin, Positive Pion-Proton Scattering at the Energies 176, 200, 270, 307, and 310 MeV, from Proceedings of the CERN Symposium on High-Energy Accelerators and Pion Physics, Vol. II (CERN, Geneva, 1956), p. 204.

6. J. Ashkin, Nuovo Cimento Suppl. 14, Ser. X, No. 2, 221 (1959).

7. J. H. Foote, O. Chamberlain, E. H. Rogers, and H. M. Steiner, Phys. Rev. 122, 959 (1961).

8. E. Fermi, N. Metropolis, and E. F. Alei, Phys. Rev. 95, 1581 (1954).

9. H. L. Anderson, W. C. Davidon, M. Glicksman, and V. E. Kruse, Phys. Rev. 100, 279 (1955).

10. H. R. Rugge and O. T. Vik, Phys. Rev. 129, 2300 (1963);
O. T. Vik and H. Rugge, Phys. Rev. 129, 2311 (1963).

11. L. D. Roper, Phys. Rev. Letters 12,340 (1940).

12. A. Donnachie, J. Hamilton, and A. T. Lea, Phys. Rev. 135, B515 (1964).

13. Y. S. Kim, Phys. Rev. 129, 862 (1963).

Table I. Description of counters

Item	Size (in.)	Thickness (in.)
S_1	5 x 5	3/16
S_2	2-1/2 diam	3/16
S_3	5 x 5	3/16
S_4	7 x 13	1/4
S_5	10 x 20	1/4
C	4-1/2 diam	2-3/8

Table II. Summary of the raw data, the applied corrections, and the corrected data.

θ_{LAB} (deg.)	Counter geometry	Raw Data $(S_1S_2C)_{NET}$ (counts/volt)	Fraction of counts due to protons fp (%)	Overall Cerenkov efficiency, ϵ (%)	Doubles rate $(S_1S_2)_M$ (counts/volt)	Net fraction of pions lost by scattering and decay, f (%)	Geometrical correction, g	Corrected data $\frac{(S_1S_2C)_{NET}(1-f_p)}{(1-f)\,\epsilon\,g}$ (counts/volt)
11.0	LA	1999.8±89.4	1.97±0.18	97.35±0.07	2013.8±92.0	+4.06±0.08	0.998	2103.2±96.1
14.8	LA	1755.3±47.6	1.98±0.12	97.31±0.08	1768.2±49.0	+4.11±0.08	0.998	1847.6±51.2
22.3	LA	1410.0±31.2	1.84±0.09	97.19±0.08	1424.0±32.0	+4.28±0.08	0.999	1489.8±33.5
22.3(a)	LA	1511.7±75.7	1.77±0.18	97.22±0.08	1527.4±77.9	+2.96±0.08	0.999	1576.2±80.4
22.3	SA	1454.8±13.8	1.84±0.07	97.[illegible]±0.08	1471.9±14.3	+2.83±0.08	0.994	1524.1±14.7
37.7	SA	866.2± 5.2	0.76±0.29	96.54±0.10	890.4± 6.1	+2.69±0.09	0.996	918.3± 6.3
54.2	SA	407.0± 4.8		95.60±0.11	425.7± 5.0	+2.83±0.11	1.000	438.2± 5.2
72.2	SA	176.4± 2.8		93.85±0.14	188.0± 3.0	+0.77±0.20	1.003	188.8± 3.0
90.0(b)	SA				154.3± 2.7	-0.52±0.37	1.000	153.5± 2.7
92.1	SA	137.4± 1.8		91.69±0.24	149.9± 2.0	-0.52±0.37	1.000	149.1± 2.1
114.4	SA	182.7± 3.6		87.78±0.34	209.6± 3.2	-0.24±0.27	0.997	209.7± 3.2
126.5	SA	198.7± 3.9		84.23±0.43	235.4± 4.6	+0.03±0.24	0.997	236.2± 4.6
139.2(b)	SA				265.1±13.7	-0.30±0.22	0.997	265.1±13.7
149.8(b)	SA				271.0± 5.1	-0.56±0.20	0.997	270.3± 5.1
152.5	SA	205.0± 3.9		72.39±0.72	283.2± 6.1	-0.64±0.20	0.997	282.2± 6.1

(a) These data were taken with a separation of 20.25 in. between S_1 and S_2.

(b) The doubles rate $(S_1S_2)_M$ was measured directly at these angles and at 114.4 deg., 126.5 deg. In the last two cases it was combined with the data derived from $(S_1S_2C)_{NET}$.

Table III. Experimental π^+-p differential cross section in the center-of-mass system.[a]

θ^* (deg)	$\frac{d\sigma}{d\Omega^*}$ (mb/sr)	Relative error (%)
14.9	27.52 ± 1.26	4.6
20.0	24.46 ± 0.68	2.8
30.0	20.80 ± 0.18	0.9
49.9	13.927± 0.095	0.7
69.9	7.730± 0.093	1.2
89.9	3.930± 0.062	1.6
107.9	3.995± 0.069	1.7
109.9	3.969± 0.054	1.4
130.0	6.986± 0.107	1.5
140.0	8.73 ± 0.17	1.9
150.0	10.71 ± 0.55	5.1
158.0	11.57 ± 0.22	1.9
160.0	12.23 ± 0.26	2.1

[a]There is a 3% uncertainty in the absolute scale of the differential cross section.

Table IV. Polarization of the recoil proton for $\pi^{\pm}$p scattering in the center-of-mass system.

θ (deg)	P(θ)
68.0	0.290 ± 0.138
80.5	0.380 ± 0.126
108.4	0.219 ± 0.064
119.1	-0.035 ± 0.075
129.1	0.033 ± 0.068
138.0	-0.067 ± 0.062
147.0	-0.156 ± 0.072

Table V. Phase-shift solutions.

1. SPD phase-shift solution

Solution	Nuclear phase shifts					χ^2 (Expected: 15)		
	$S_{3,1}$	$P_{3,1}$	$P_{3,3}$	$D_{3,3}$	$D_{3,5}$	Total	DCS[a]	POL[a]
Fermi-I	-18.3±0.6	-7.3±0.6	118.9±1.3	0.9±0.6	-1.9±0.6	15.5	11.6	3.9

2. SPDF phase-shift solutions

Solution	Nuclear phase shifts							χ^2 (Expected: 13)		
	$S_{3,1}$	$P_{3,1}$	$P_{3,3}$	$D_{3,3}$	$D_{3,5}$	$F_{3,5}$	$F_{3,7}$	Total	DCS[a]	POL[a]
A	-18.4±0.7	-8.0±1.6	119.3±1.3	0.0±1.6	-1.3±1.3	0.0±0.8	0.6±1.0	13.3	8.9	4.4
B	-18.7	-12.2	153.2	2.3	-24.6	-4.1	21.0	20.1	13.1	7.0
C	-37.6	-13.9	146.5	-13.5	21.5	-0.7	-3.4	22.8	7.7	15.1

(a) These columns list the contributions to the total χ^2 from the differential cross section (DCS) and the recoil-proton polarization (POL).

Table VI. Tables of Error Matrices for SPD and SPDF Solutions

Matrix I. Error matrix G^{-1} for the SPD Fermi-I solution (in deg^2).

	$S_{3,1}$	$P_{3,1}$	$P_{3,3}$	$D_{3,3}$	$D_{3,5}$
$S_{3,1}$	0.42	0.29	0.61	0.17	-0.17
$P_{3,1}$		0.37	0.43	0.16	-0.19
$P_{3,3}$			1.57	0.00	0.07
$D_{3,3}$				0.33	-0.26
$D_{3,5}$					0.32

Matrix II. Error matrix G-1 for the SPDF solution A (in deg^2).

	$S_{3,1}$	$P_{3,1}$	$P_{3,3}$	$D_{3,3}$	$D_{3,5}$	$F_{3,5}$	$F_{3,7}$
$S_{3,1}$	0.48	0.76	0.40	0.66	-0.54	0.26	-0.36
$P_{3,1}$		2.68	-0.38	+2.44	-1.97	1.11	-1.61
$P_{3,3}$			1.84	-0.71	0.68	-0.34	0.49
$D_{3,3}$				2.53	-1.99	1.05	-1.57
$D_{3,5}$					1.69	-0.84	1.22
$F_{3,5}$						0.57	-0.74
$F_{3,7}$							1.10

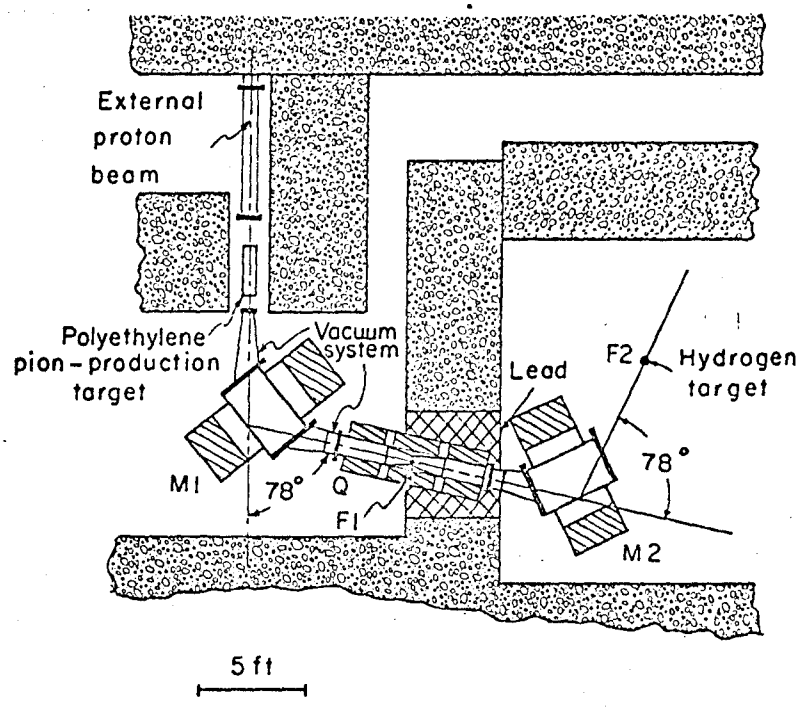

Fig. 1. Plan view of the pion-beam spectrograph.

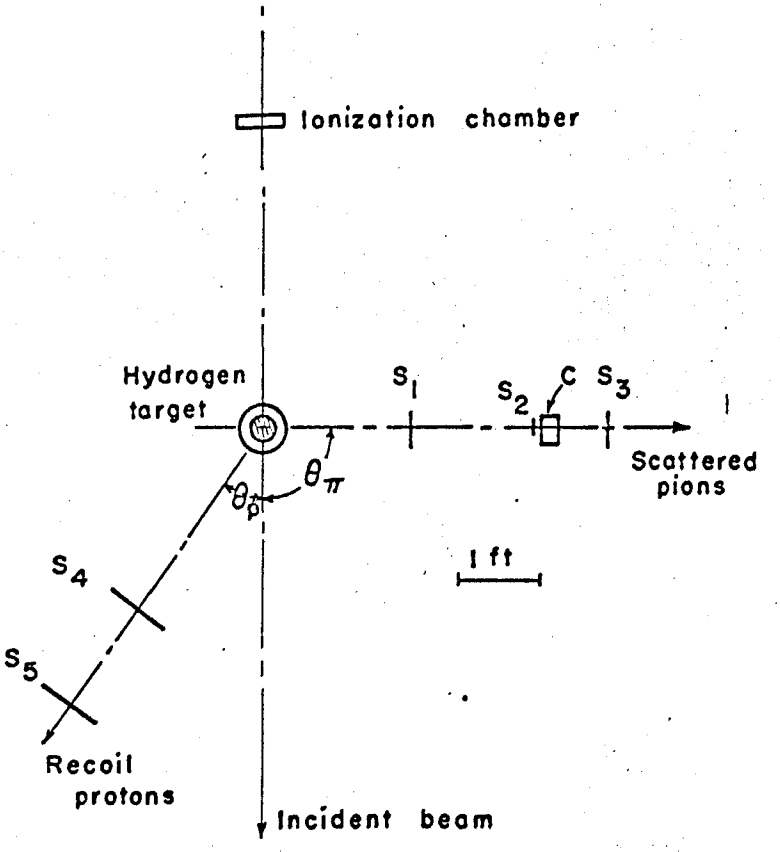

Fig. 2. Scale drawing of the counter telescopes.

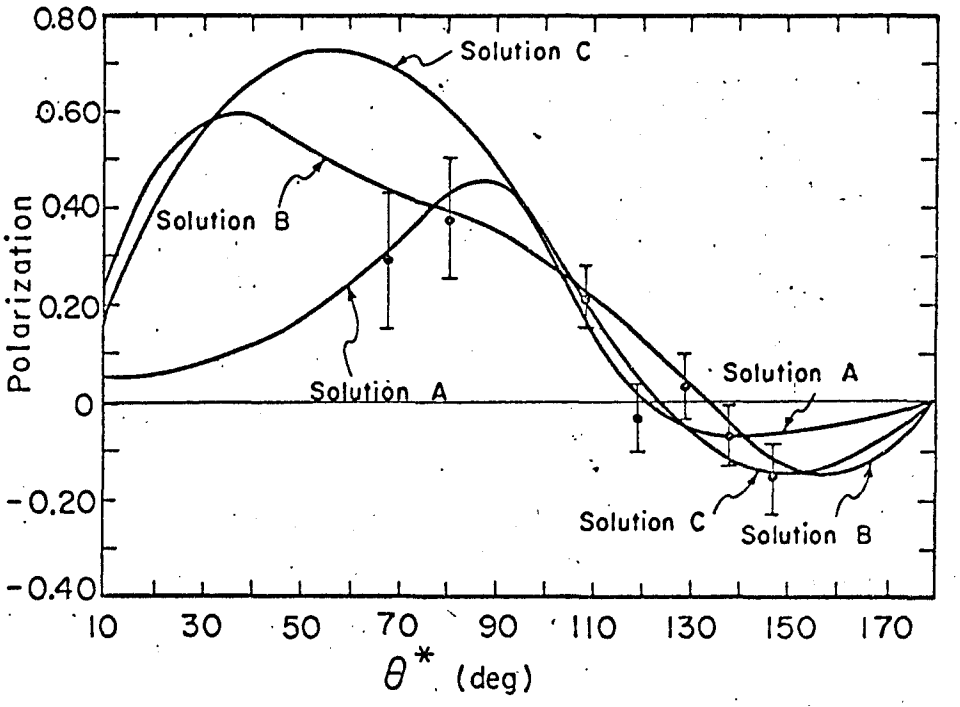

Fig. 3. Recoil-proton polarization data and the corresponding values calculated from the three SPDF phase-shift solutions.

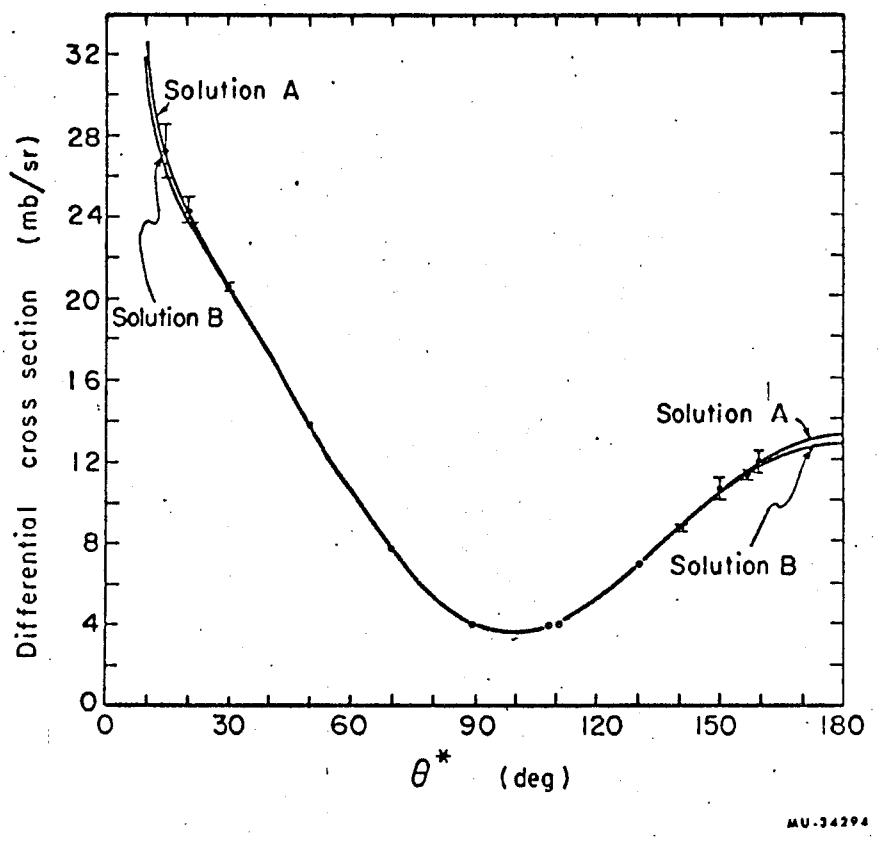

Fig. 4 Comparison between the fits to the experimental data of the differential cross sections based on the phase shifts of SPDF solution A and solution B.